JMEPEG (2020) 29:167–174
https://doi.org/10.1007/s11665-019-04551-9

1059-9495/$19.00

The Effect of Acid Pickling on the Corrosion Behavior of a Cerium Conversion-Coated AA2198-T851 Al-Cu-Li Alloy

Rafael Emil Klumpp, Uyime Donatus, João Victor S. Araujo, Marcelo Myada Redígolo, Caruline de S.C. Machado, and Isolda Costa

(Submitted March 31, 2019; in revised form November 28, 2019; published online January 8, 2020)

The effect of acid pickling pretreatments prior to cerium conversion coating process on the corrosion behavior of AA2198-T851 alloy substrates was investigated. Three acid pretreatments were employed: nitric acid (HNO_3), phosphoric acid (H_3PO_4) and sulfuric acid (H_2SO_4). The cerium conversion coating process was performed using a batch solution composed of cerium nitrate and hydrogen peroxide. Microscopic techniques, electrochemical impedance spectroscopy, polarization resistance and open-circuit potential measurements were employed to investigate the effect of each acid pretreatment. The untreated and nitric acid pretreated substrates presented more defective cerium conversion layers than the substrates treated with phosphoric and sulfuric acids. Accordingly, the corrosion resistance of the untreated and nitric acid-treated substrates was very low, while that of the substrates treated with phosphoric acid and sulfuric acids were greatly improved. The sulfuric acid pickling treatment was the best pretreatment before cerium conversion coating among the investigated pretreatments on the AA2198-T851 Al-Cu-Li alloy.

Keywords Acid pickling, Al-Cu-Li alloy, cerium conversion coating

1. Introduction

Cerium-based conversion coatings have been considered promising alternatives for replacing carcinogenic hexavalent chromium layers for the protection of metals, particularly Al alloys (Ref 1-5).

The cerium conversion coating process starts with the electrochemical reactions that are responsible for the formation and growth of cerium oxide layers on the surfaces of treated alloys (Ref 1, 6, 7). These reactions are caused by surface activation with the formation of microcells on surface defects, such as grain boundaries, precipitates, inclusions or submicroscopic cracks in the metal oxide layer. The pH increase near the active surface and the precipitation of a hydrated oxide layer starts the subsequent oxide film formation, according to reactions 1-4 (Ref 1, 7, 8):

$$Al^{\circ} \rightarrow Al^{3+} + 3e^{-} \quad \text{(Eq 1)}$$

$$O_2 + 2H_2O + 4e^{-} \rightarrow 4OH^{-} \quad \text{(Eq 2)}$$

$$2Ce^{3+} + 2H_2O_2 + 8OH^{-} \rightarrow 2Ce(OH)_4 + 2H_2O + O_2 + 2e^{-} \quad \text{(Eq 3)}$$

$$Ce(OH)_4 \rightarrow CeO_2 + 2H_2O \quad \text{(Eq 4)}$$

According to this mechanism, the use of oxidizing agents, such as hydrogen peroxide shown in reaction 5, accelerates the deposition of cerium products by oxidizing Ce^{3+} to Ce^{4+} (Ref 1, 7, 8). In a review paper by Harvey (Ref 1), it was explained that hydrogen peroxide (H_2O_2) acts simultaneously as an oxidizing agent, crystallization inhibitor and an hydroxyl source (Ref 7, 9).

Cerium-based conversion coatings require pretreatment prior to the deposition of the cerium oxide layer (Ref 1). The surface preparation has a strong influence on cerium deposition and coating performance (Ref 1). It increases the coating deposition rate by exposing the subsurface (often Cu or Fe rich) and accelerates the cathodic deposition (Ref 1). Many acids are used as pretreatments, including HF, HNO_3, H_2SO_4-HF and H_2SO_4-H_3PO_4. The literature reports that treatment with H_2SO_4-H_3PO_4 does not affect the electrochemical behavior of intermetallic particles in the matrix of treated alloys (Ref 1).

Many authors have reported success with the use of a cerium-based conversion coating as an anticorrosion agent for different Al alloys (Ref 1, 5, 8, 10-14). However, reports on the corrosion behavior of cerium conversion layers on the next generation of Al-Cu-Li alloys are scarce. These alloys find application in the aerospace industry due to their weight reduction and increase in elastic modulus due to the addition of lithium (Ref 13). The AA2198-T851 alloy employed in this study is a representative member of the next generation of Al-Cu-Li alloys. These alloys are susceptible to localized corrosion that has been mainly associated with T1 phase (Al_2CuLi), which is located preferentially in regions of high dislocation density due to intense deformation (Ref 13). Reports detailing the corrosion mechanism of AA2198-T851 were published by Donatus et al. (Ref 14) and Araujo et al. (Ref 15, 16). These authors revealed that the predominant mode of corrosion in this alloy is intragranular, and it propagates through bands parallel to the {111} Al planes. These bands are rich in the hexagonal

Rafael Emil Klumpp, Uyime Donatus, João Victor S. Araujo, Marcelo Myada Redígolo, Caruline de S.C. Machado, and **Isolda Costa**, Instituto de Pesquisas Energéticas e Nucleares, Av. Prof. Lineu Prestes, 2242, São Paulo, Brazil. Contact e-mail: rafahemil@hotmail.com.

T1 (Al_2CuLi) phase, which is the phase of foremost concern with respect to the corrosion resistance of Al-Cu-Li alloys (Ref 14-17).

Given that the Al-Cu-Li alloys are highly susceptible to corrosion, these alloys are often protected against corrosion. However, to obtain an efficient cerium coating on the alloy, pretreatments of the as-received surface have to be carried out prior to the application of cerium conversion coatings.

Acid pretreatments have a strong influence on the conversion coating process of this alloy. In essence, the pretreatment significantly affects the layer formation, morphology and corrosion behavior of the AA2198-T851 alloy. Thus, the focus of the present study is to investigate and compare selected commonly used acids, namely HNO_3, H_3PO_4 and H_2SO_4, with the aim of choosing the one with the optimal corrosion performance after cerium conversion coating on the AA2198-T851 alloy.

2. Experimental Methods

An AA2198-T851 alloy (composition of Cu 3.31 wt.%, Li 0.96 wt.%, Mg 0.31 wt.%, Si 0.03 wt.%, Fe 0.04 wt.%, Ag 0.25 wt.%, Zr 0.4 wt.%, Zn 0.01 wt.% and Al balance—determined by inductive couple plasma technique) was employed in this study.

Four sets of substrates were prepared from the AA2198-T851 alloy using different acid pickling pretreatments. Prior to the acid pickling pretreatments, all the samples were first degreased in ethanol. The first set of substrates (designated as NP) was pickled in 4 mol L-1 HNO_3 solution; the second set (designated as PP) was pickled in 4 mol L^{-1} H_3PO_4 solution; the third set (designated as SP) was pickled in 4 mol L^{-1} H_2SO_4 solution; and the fourth set was used as a control (designated as C) and only degreased in ethanol. All acid pickling pretreatments were carried out for 2 h. After these pretreatment operations, the substrates were rinsed with deionized water for 30 s followed by a cerium conversion coating process and a final rinse in deionized water.

The cerium conversion coating process was carried out using a cerium (III) nitrate solution comprising 0.015 mol L^{-1} hydrated $Ce(NO_3)_3$ + 0.029 mol L^{-1} H_2O_2 at 4.5 pH and deionized water until 1 L of solution was produced (Ref 4). The four sets of substrates (as explained above) were treated by immersion in the cerium (III) nitrate solution for 30 min at 37 °C and then oven-dried at 105 °C for 10 min.

Corrosion studies were conducted in a 3.5 wt.% NaCl solution using electrochemical impedance spectroscopy (EIS) technique with a Gamry Potentiostat. A three-electrode setup, comprising the working electrode, Pt counter electrode and an Ag/AgCl (saturated KCl) reference electrode, was used for the experiments. The EIS measurements were carried out from 50 kHz to 10 mHz with an amplitude of perturbation of 10 mV relative to the OCP, and the data were collected at a rate of 10 points per decade. The open-circuit potential (OCP) measurements were obtained in each acid pretreatment solution for two hours of exposure using the same apparatus described earlier for EIS measurements.

Scanning electron microscopy (SEM) was performed using a JEOL JSM 6010 microscope equipped with an energy-dispersive X-ray spectroscopy (EDS) detector.

3. Results and Discussion

To understand the effect of the acid pretreatment on the cerium-based conversion coating and, consequently, on the corrosion behavior of the AA2198-T851 alloy, the microstructures of the pretreated substrate surfaces were examined. The results were then correlated with the electrochemical and corrosion responses of the alloy for each acid pretreatment.

3.1 Microstructure Analysis

Figure 1 shows the SEM image of the AA2198-T851 alloy in the as-received condition (designated as C) without acid pretreatment but treated in the cerium conversion coating solution. The figure displays the morphology expected for a cerium conversion coating with cracks in the formed layer. Defects of this type in conversion layers have been reported since the first studies with cerium-based conversion layers (Ref 1, 8, 18). These are regions with an increased tendency for the initiation of localized corrosion. This phenomenon has also been observed by many authors (Ref 1, 3). Figure 1 shows that the cracks propagate through the parallel bands. These bands are enriched in Mg, as already presented in previous works from the same group (Ref 14, 15). Clearly, the presence of Mg enrichment (primarily in the bands) on the surface of the alloy has a negative impact on the cerium conversion coating.

The SEM image of the NP (nitric acid pickled) substrate is shown in Fig. 2. This figure also shows the morphology after a cerium conversion coating process where cracking is observed. In Fig. 2, it is important to note that cracks are seen all over the surface and are not aligned in the bands, as observed in sample C (Fig. 1). The surface of the NP (nitric acid pickled) samples presents an increased tendency for localized corrosion initiation since it contains many pre-attacked and cracked regions. Figure 3 shows the details of the defects in the uncovered areas. In these areas, the exposure of the bare metal substrate is observed. These regions correspond to areas with an increased tendency for the initiation of localized corrosion.

Figure 4 shows SEM image of the substrate subjected to the PP (phosphoric acid pickled) process. The morphology of the cerium conversion coating is far less defective, as shown in Fig. 4, than those of the C (without pickling) and NP (nitric acid pickled) substrates. In Fig. 4, however, cracks are observed. A less defective coating provides an improved

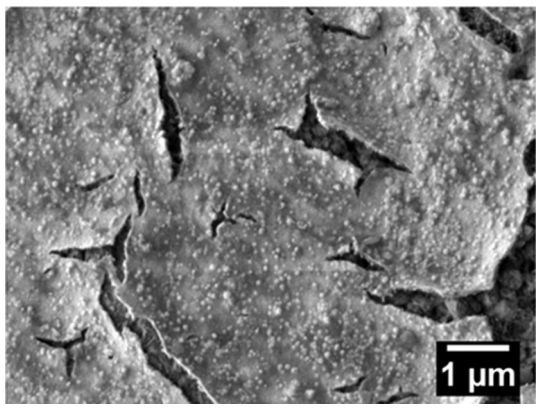

Fig. 1 SEM image of the AA2198-T851 without acid pickling (C) after cerium conversion coating treatment

barrier effect and, consequently, increases the corrosion resistance of the coated sample.

Figure 5 presents SEM images of the substrate subjected to SP treatment (sulfuric acid pickled). Similar to the PP substrate (phosphoric acid pickled), this image shows a cerium conversion coating layer that is less defective than that on the C (without acid pickling) and NP (nitric acid pickled) substrates. Figure 5 also shows that the formed layer on the SP sample is slightly more homogenous and less defective than that on the PP (phosphoric acid pickled) sample.

Figure 6 presents SEM images of the cross sections of the Al alloy samples after cerium conversion coating. Figure 6(a) is that of the AA2198-T851 alloy in the as-received condition without acid pickling (designated as C), as shown in Fig. 1. This image shows a cerium conversion coating layer that is very defective, with uncovered areas. The cross section of the NP (nitric acid pickled), presented in Fig. 6(b), also shows a defective layer with uncoated areas. Figure 6(c) shows the cross section of the Al alloy exposed to the PP (phosphoric acid pickling) process. The morphology of the cerium conversion coating layer on the PP sample is also highly defective, with uncoated areas. However, it is not as defective as that of the C and NP (in Fig. 6a and b) samples. The cross-section SEM images of the substrate subjected to the SP treatment (sulfuric acid pickled) are displayed in Fig. 6(d), which shows a cerium conversion coating layer that is less defective than that of all the other surfaces tested herein.

Figure 7 shows the areas/points where EDS analysis was carried out, and the results are presented in Tables 1, 2, 3 and 4. The results suggest a layer comprising a mixed oxide of Al and Ce with the morphology presented in Fig. 1. The semiquantitative compositions of the points analyzed for the AA2198-T851 sample without pickling are shown in Table 1. A comparatively increased cerium content is related to the areas with increased oxygen content and decreased aluminum concentration. Additionally, the highest Ce contents herein

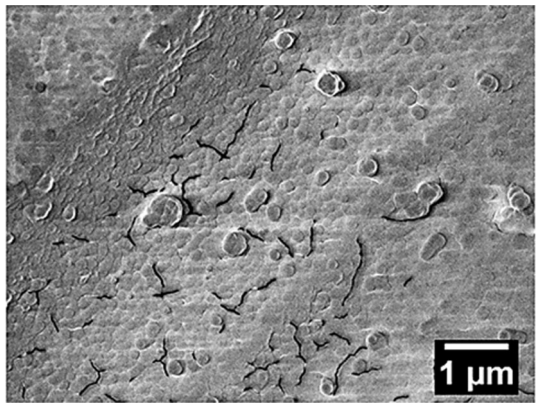

Fig. 4 SEM image of the AA2198-T851 alloy phosphoric acid pickled (PP) after cerium conversion coating treatment

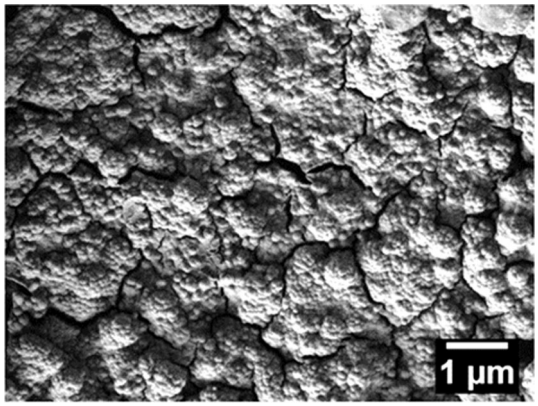

Fig. 2 SEM image of the AA2198-T851 alloy with nitric acid pickled (NP) after cerium conversion coating treatment

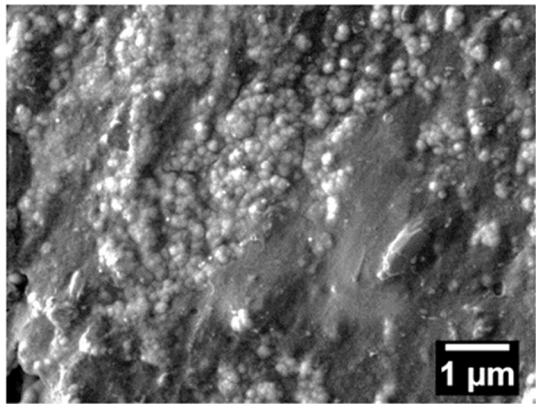

Fig. 5 SEM image of the AA2198-T851 alloy sulfuric acid pickled (SP) after cerium conversion coating treatment

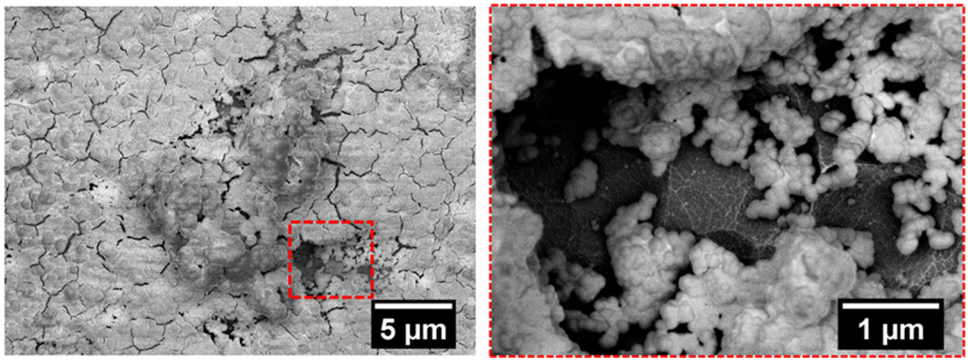

Fig. 3 SEM images showing a defected area on the nitric acid pickled (NP) substrate after cerium conversion coating treatment

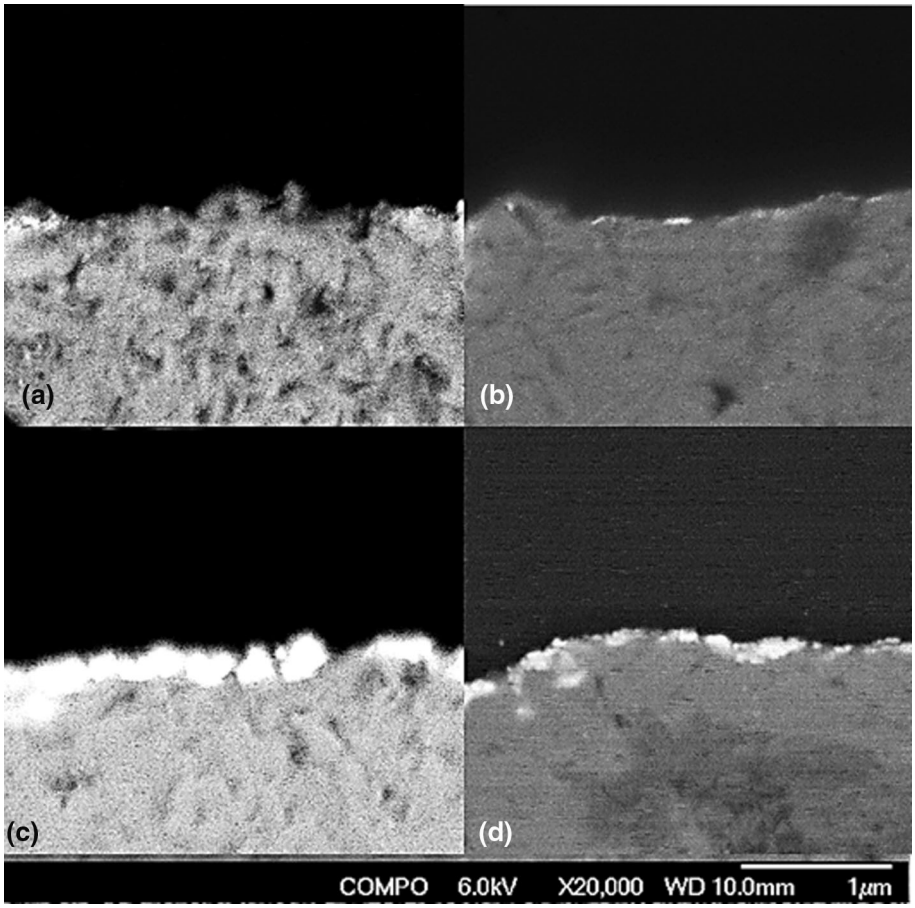

Fig. 6 SEM images of the cross section after cerium conversion coating: (a) C, without acid pickling; (b) NP, nitric acid pickled; (c) PP, phosphoric acid pickled (d) and (e) SP, sulfuric acid pickled

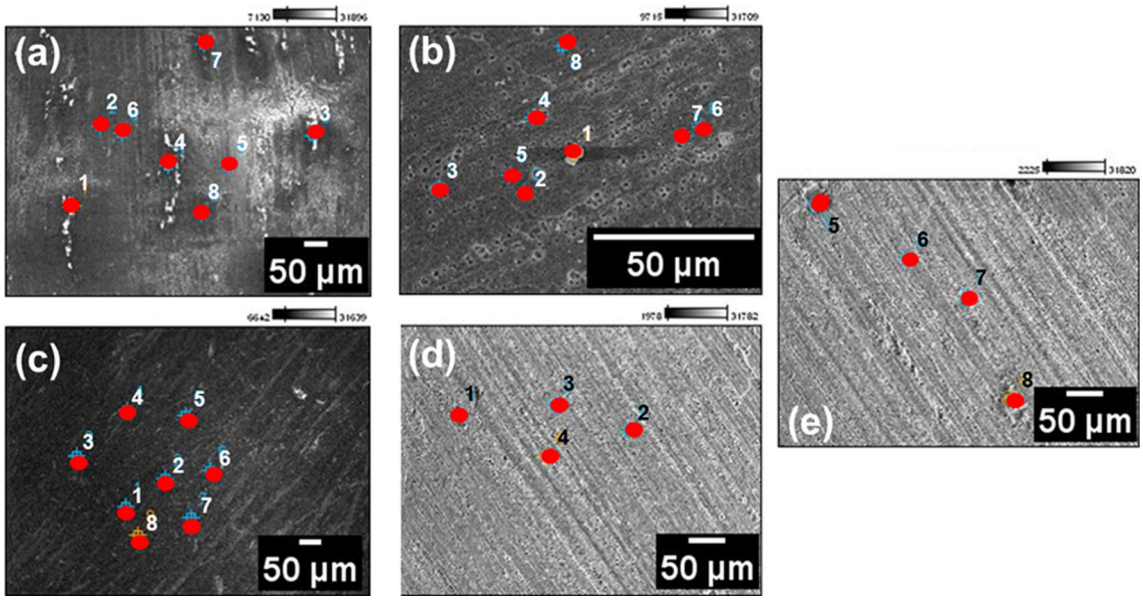

Fig. 7 SEM showing the areas where EDS analysis was carried out: (a) C, without acid pickling; (b) NP, nitric acid pickled; (c) PP, phosphoric acid pickled (d) and (e) SP, sulfuric acid pickled

are seemingly associated with the presence of silicon. It is important to note that in the areas where Cu is found, the Ce content decreased. This result suggests that Ce oxide was mainly deposited on Cu rich particles that acted as cathodic sites where pH was preferentially increased leading to precipitation of Ce hydroxide and subsequently formed Ce oxide. The

distribution of Ce is not homogenous, and a concentration ranging from 3.14 to 19.38 wt.% is estimated. In the areas with relatively high copper contents, the cerium content is between 3.14 and 5.14 wt.%, whereas in the other areas, this content varies from 9.07 to 19.38% wt.%. It is interesting to observe that Mg peaks are not observed (or not intense) in the EDS spectra. The absence of Mg suggests that it was consumed during the conversion coating treatment. It must be mentioned that EDS cannot detect Li.

The EDS spectra analysis of the NP (nitric acid pickled and with Ce conversion coating) sample also presents peaks for O, Al and Ce, but it is important to note that the Ce peaks are more evident for this kind of surface than for that without acid pickling (C). As presented in Table 2, the Ce content in the NP sample varies from 0.06 to 57.34 wt.%, showing a larger variation in Ce concentration than that obtained from the C sample. It is also interesting to note that the distribution of Ce is very heterogeneous, as evident from the significant differences in the weight percentages obtained from the different points on the NP (nitric acid pickled) surface. These results indicate that there is a strong pickling process influence on the Ce conversion treatment and that it is in accordance with the morphology presented in Fig. 2, which shows a very defective layer.

The EDS composition analysis presented in Tables 3 and 4 suggests a more uniform Ce distribution on the surfaces of the PP (phosphoric acid pickled) and SP (sulfuric acid pickled) samples, respectively. This is in accordance with a less defective morphology related to these two treatments than the others considered herein, as presented in Fig. 4 and 5, i.e., improved distribution of Ce species was achieved as a result of very homogenous surfaces. The formation and growth of a mixed Al and Ce oxide layer on the Al alloy surface start with cathodic reactions (microcells) on the exposed substrate at surface defects (Ref 1, 7, 8, 19). A very active and heterogeneous surface (with more defects) experiences more heterogeneous precipitation of a hydrated oxide layer and oxide film formation. It is important to note that in both types of pickling treatments, PP and SP, the distribution of Al, O, Cu and Ce is similar. Cu is seen at all points in the concentration range between 1.09 and 7.03 wt.%, but this is not the case for the C (without acid pickling) and NP (nitric acid pickled) pretreated samples.

Table 1 Semiquantitative chemical composition (wt.%) analyzed by EDS of the AA2198-T851 without acid pickling (C) and with cerium conversion coating treatment

Without pickling	O-K	Al-K	Si-K	Cu-K	Ce-L
pt1	40.48	40.14			19.38
pt2	9.00	83.52		2.97	4.51
pt3	45.59	38.49	0.96		14.97
pt4	51.34	37.25	0.77		10.63
pt5	5.75	88.09		3.02	3.14
pt6	7.83	85.34		2.72	4.10
pt7	53.58	36.99	0.39		9.04
pt8	12.62	78.65		3.17	5.57

Table 3 Semiquantitative chemical composition (wt.%) by EDS of the PP (phosphoric acid pickled) AA2198-T851 after cerium conversion coating

Pickling in H_3PO_4	O-K	Al-K	Cu-K	Ce-L
pt1	14.85	65.95	2.47	16.73
pt2	14.67	67.38	2.68	15.28
pt3	11.60	70.96	3.23	14.22
pt4	7.28	73.85	7.30	11.58
pt5	11.58	68.44	3.23	16.75
pt6	12.68	63.22	3.78	20.33
pt7	16.42	56.56	2.92	24.10
pt8	10.18	68.87	3.09	17.87

Table 4 Semiquantitative chemical composition (wt.%) by EDS of the SP (sulfuric acid pickled) AA2198-T851 after cerium conversion coating

Pickling in H_2SO_4	O-K	Al-K	Cu-K	Ce-L
pt1	16.21	57.78	2.71	23.29
pt2	15.81	64.23	2.53	17.43
pt3	8.92	79.29	1.02	10.76
pt4	17.40	60.24	3.25	19.11
pt5	20.55	57.21	2.19	20.05
pt6	12.55	68.10	3.49	15.86
pt7	12.39	70.35	2.92	14.35
pt8	11.00	74.11	2.80	12.09

Table 2 Semiquantitative chemical composition (wt.%) of the AA2198-T851 pretreated by nitric acid pickling (NP) and coated with Ce conversion coating and analyzed by EDS

Pickling in HNO_3	O-K	Al-K	Si-K	Fe-K	Cu-K	Zr-L	Ce-L
pt1	35.78		0.58	63.57			0.06
pt2	30.17	8.69				3.81	57.34
pt3	4.53	66.77					28.70
pt4	6.82	67.77					25.41
pt5	12.87	70.25			2.81		14.07
pt6	16.17	64.33			2.59		16.91
pt7	22.69	19.99					57.32
pt8	9.80	76.03			5.56		8.61

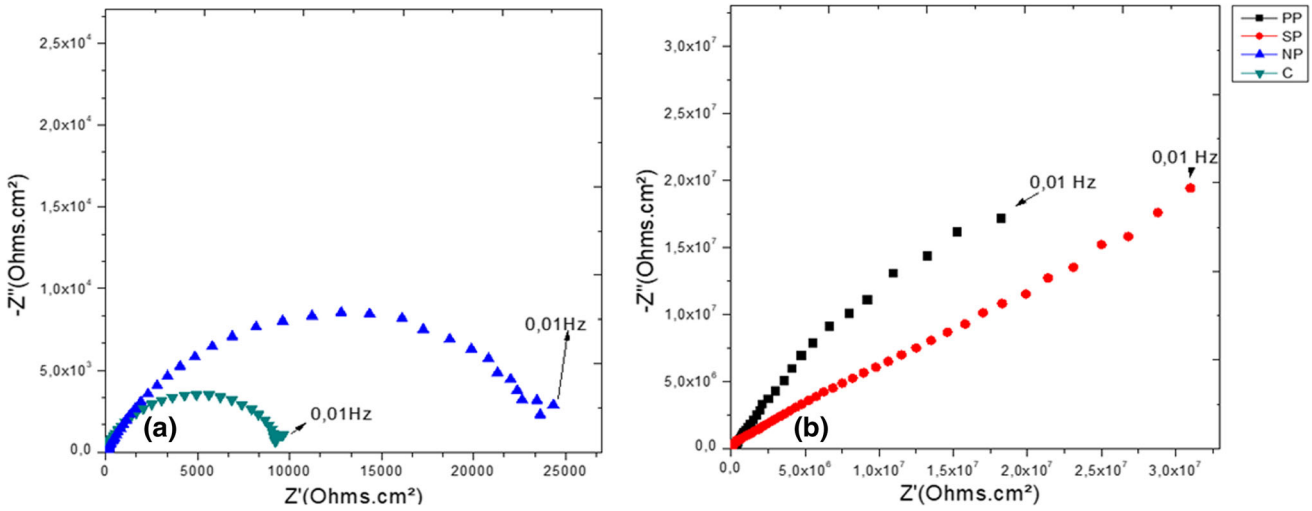

Fig. 8 EIS results for the AA2198-T851 alloy with cerium conversion coating after 24 h in 3.5 wt.% NaCl solution. Nyquist diagrams of (a) samples C (without acid pickling) and NP (nitric acid pickled), and (b) samples pickled in phosphoric acid (PP) and sulfuric acid (SP)

3.2 Electrochemical Testing

EIS measurements of the differently pretreated samples are compared in Fig. 8. The measurements were obtained after immersion for 24 h in the 3.5 wt.% NaCl solution. In the Nyquist plots (Fig. 8a), the spectra of C and NP samples are separated from those of PP and SP ones (Fig. 8b) because the impedances of the latter are far higher and overwhelmed those of the C and NP when plotted together. The Nyquist diagrams corresponding to C, NP and PP show flattened capacitive loops, due to the heterogeneous surface layer and the interaction of the time constants related to the defective conversion coatings and the substrate exposed to the electrolyte at the coating defects. The EIS results also indicated that charge transfer processes coupled with the charging of the double layer at the exposed substrate predominated the response of the defective coating for the C, NP and PP treatments. The results corresponding to the sample with sulfuric acid pickling and conversion coating present a distinguished behavior compared to the other treatments. This is typical of a porous electrode through which diffusion-controlled processes occur. The porous layer corresponds to the conversion coating with defects, as displayed in the SEM images (Fig. 6d). Highly defective layer with large amounts of cracks, especially along parallel bands, is associated with Mg enrichment (Fig. 1). The attack to the Mg-enriched layer by nitric acid pickling (NP) resulted in increased impedances (around 2.5 times larger) compared to that of the untreated one (C sample), showing that the NP (nitric acid pickled) treatment had a beneficial effect on the formation of the Ce conversion layer compared to that of the C treatment. The layer corresponding to NP treatment also shows a large number of defects, such as cracks, as illustrated in Fig. 2.

Despite the increased impedance, the magnitude for both conditions, C and NP, was in the same range. This is due to the highly defective characteristic of the conversion layer on both substrates, C and NP. These results show that pickling in an HNO_3 solution is not proper as a surface preparation treatment for cerium conversion coating on the AA2198-T851 alloy and may even be more detrimental than beneficial (due to non-uniform cerium oxide formation) when compared with the samples that were not pickled. A correlation between coating morphology (Fig. 1-6) and EIS results (Fig. 8b) shows that the higher impedances, for the PP (phosphoric acid pickled) and SP (sulfuric acid pickled) samples than those for the C and NP samples, were related to coatings with a decreased amount of defects. In fact, the SP pretreated sample presented the highest impedances of the samples studied herein, even at low frequencies. These results are in accordance with the SEM and EDS analyses, which show conversion layers with increased uniformity and homogeneity after pickling in H_3PO_4 and H_2SO_4 acid solutions. Thus, the elevated impedances were due to the improved barrier effects provided by the SP pretreatment. A comparison of the magnitude of the impedances for all types of surfaces tested shows that, for the PP (phosphoric acid pickled) and SP (sulfuric acid pickled) samples, the impedances were significantly higher—on the order of 107 Ohm.cm^2—than those for the NP (nitric acid pickled) and C (without acid pickling) samples, which were in the order of 104 Ohm.cm^2. This difference is displayed in Fig. 8 for all the investigated surfaces. There is a pronounced difference between the impedances of the tested surface, which is attributed to the characteristics of the formed layers with a decreased amount of defects on the PP (phosphoric acid pickled) and SP (sulfuric acid pickled) substrates.

In order to investigate the behavior of the pretreated surfaces for long exposure times, EIS results (shown as Z modulus versus time) of the differently pretreated samples were compared (Fig. 9). The measurements were obtained in 3.5 wt.% NaCl solution for 168 h. As discussed earlier, impedance plots of the C and NP samples were separated from those of the PP and SP samples because impedance values of the latter were far higher and overwhelmed those of the C and NP when plotted together. Figure 9(a) shows that the lowest impedances were related to the surface of the C sample, and it decreased with exposure time. The impedance results corresponding to the NP sample showed higher values compared to the C sample, and these were stable with exposure time. Figure 9(b) shows that the PP (phosphoric acid pickled) samples revealed significantly higher impedances and fairly stable values for 168 h. However, the impedances related to the SP (sulfuric acid pickled) treatment increased with time of exposure suggesting that the products of the corrosion reaction

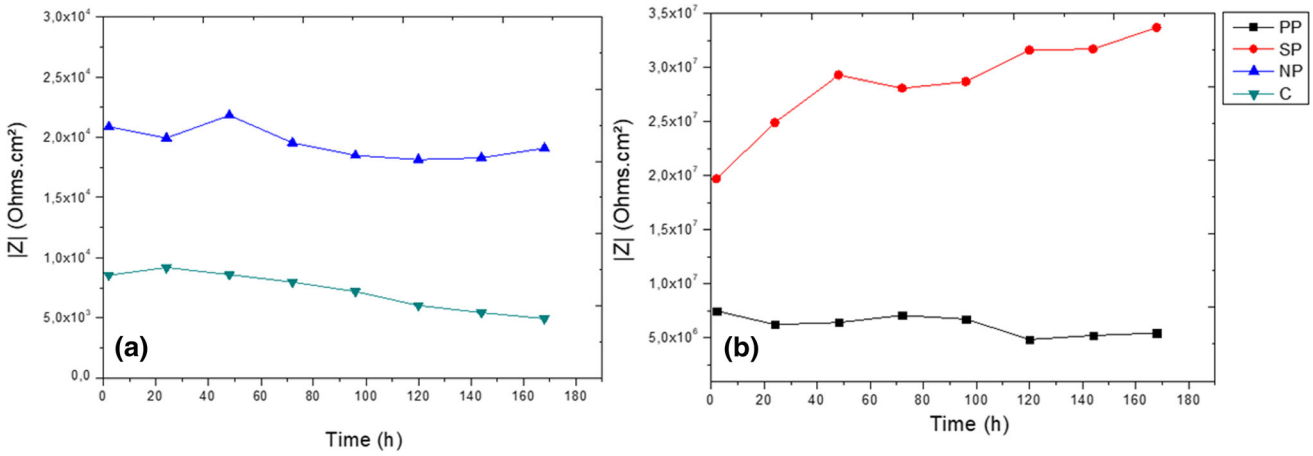

Fig. 9 EIS (modulus of Z vs. time) results for the AA2198-T851 alloy with cerium conversion coating in 3.5 wt.% NaCl solution for 168 h. (a) EIS results for samples C, without acid pickling, and NP, nitric acid pickled. (b) EIS results for samples pickled in phosphoric acid (PP) and sulfuric acid (SP)

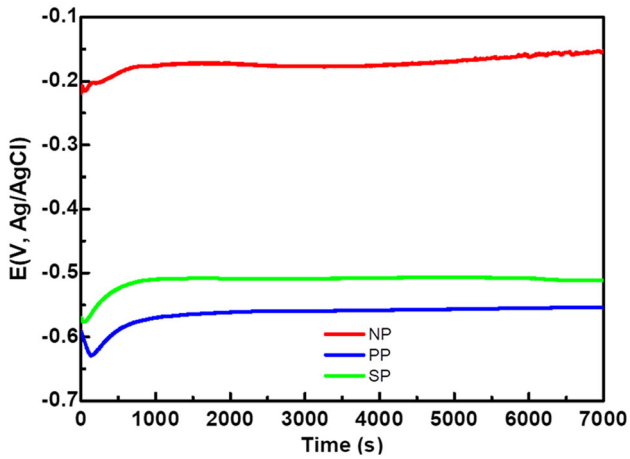

Fig. 10 Variation of open-circuit potential (OCP) as a function of time of exposure to the acids used for pickling the surface of AA2198-T851 alloy as a surface preparation step for cerium conversion coating treatment

with the environment exhibited a protective effect against the corrosion of the substrate. This result could be due to blockage of defects on the SP (sulfuric acid pickled) samples by the products of corrosion reaction.

OCP measurements of the AA2198-T851 alloy in the pickling solutions were carried out for 2 h, and the results are presented in Fig. 10. The OCP values are ranked according to the strength of the acids. The noblest potential is related to the Al alloy sample in nitric acid (HNO_3) solution. This is a strong acid with a high dissociation constant (Ref 20), meaning a high concentration of H+, (Eq 5) and high acidity on the surface of the AA2198-T851 alloy. It is important to note that in the first 30 s, the OCP reaches a minimum value that could be attributed to the attack of the thin air-formed Al2O3 layer, but subsequently, OCP values increased again. The nobler OCP values in HNO_3 (− 0.18 V) than those in H_2SO_4 (− 0.52 V) and H_3PO_4, (− 0.57 V) could be explained by the effects of NO3- in the nitric acid solution. This anion acts as a cathodic depolarizer and polarizes the anodic reaction, shifting the potential (OCP) to nobler values (Ref 21). The less noble OCP values related to H_2SO_4 solution compared to HNO_3 are associated with the strength of the first acid (H_2SO_4), which is a polyprotic acid with the first ionic acid dissociation constant (K_{a1}) $\geq$ 1 that is typical of a strong acid. The second ionic acid dissociation constant (K_{a2}) is 1.2×10^{-2}, according to Eq 6 and 7 (Ref 20). The sulfate anion (SO_4^{2-}) is a cathodic depolarizer, but its acid dissociation constant (K_{a2}) is lower than that related to NO_2^-, and thus, it causes a lower shift in the corrosion potential compared to this last anion:

$$HNO_3 + H_2O \rightarrow H_3O^+ + NO_3^- \quad K_a \geq 1 \qquad \text{(Eq 5)}$$

$$H_2SO_4 + H_2O \rightarrow H_3O^+ + HSO_4^- \quad K_{a1} \geq 1 \qquad \text{(Eq 6)}$$

$$HSO_4^- + H_2O \rightarrow H_3O^+ + SO_4^{2-} \quad K_{a2} = 1.2 \times 10^{-2} \qquad \text{(Eq 7)}$$

As presented earlier, pickling in H_2SO_4 results in the best corrosion performance among the treatments investigated herein. This is in agreement with the work of Zhou et al. (Ref 1, 22), who found that H_2SO_4 etching of the AA7075 alloy provided good corrosion performance after cerium conversion treatment.

The surface of the samples pickled in H_3PO_4 presented a steady corrosion potential at − 0.54 V. The acid dissociation constant (K_{a1}) of this acid, which is the weakest among the acids tested herein, is the lowest (7.52×10^{-3}) and presents a polyprotic behavior, as Eq 8, 9 and 10 illustrate, and consequently, low ionization of the species is due to their low activity (Ref 17):

$$H_3PO_4 + H_2O \rightarrow H_3O^+ + H_2PO^- \quad K_{a1} = 7.6 \times 10^{-3} \qquad \text{(Eq 8)}$$

$$H_2PO_4^- + H_2O \rightarrow H_3O^+ + HPO_4^{-2} \quad K_{a2} = 6.2 \times 10^{-8} \qquad \text{(Eq 9)}$$

$$HPO_4^{-2} + H_2O \rightarrow H_3O^+ + PO_4^{-3} \quad K_{a3} = 2.1 \times 10^{-13} \qquad \text{(Eq 10)}$$

Nitric acid pickling results in a highly defective surface, and the presence of NO-3, a cathodic depolarizer, affects the

homogeneity of the cerium conversion coating, as shown in the SEM and EDS results in Fig. 2. For the phosphoric acid pickling (PP) and sulfuric acid pickling (SP) treatments, the difference in corrosion performance and morphology indicates that the removal of Mg-rich bands is more effective in H_2SO_4 (SP) than in H_3PO_4 (PP). This was due to the stronger acid dissociation constant (K_{a1}) related to H_2SO_4 than that associated with H_3PO_4. Consequently, SP provides a very homogeneous surface for the cerium conversion coating process, as presented earlier by the SEM, EDS and EIS results.

4. Conclusions

The effect of acid pickling pretreatment prior to cerium conversion coating on the corrosion of the AA2198-T851 alloy was investigated. The acidic nature of the pickling had a strong influence on the cerium conversion coating homogeneity and, consequently, on the corrosion performance. Acid pickling prior to cerium conversion coating treatment improved the coating homogeneity and, consequently, the integrity of the cerium conversion layer and corrosion performance of the AA2198-T851 alloy. Sulfuric acid pickling provided the best surface condition for the cerium conversion coating and, consequently, the best corrosion resistance of the coated AA2198-T851 samples when compared with those subjected to the phosphoric or nitric acid pickling.

Acknowledgments

The authors are grateful to FAPESP (Proc. 2013/13235-6) for financial support for this research, CNPq (2017-9/169569) for the grant of João Victor de Sousa Araujo, FAPESP (2017/03095-3) for the Grant of Dr. Uyime Donatus and CAPES PROEX (88882.333459/2019-01) for the grant of Caruline de Souza Carvalho Machado. Acknowledgments are also due to the Materials Science and Technology Center of IPEN (Nuclear and Energy Research Institute) in Sao Paulo, Brazil, for SEM analysis.

References

1. T.G. Harvey, Cerium-Based Conversion Coatings on Aluminium Alloys : A Process Review, *Corros. Engeening. Sci. Technol.*, 2013, **48**(4), p 248–269
2. A. De Nicolò, L. Paussa, A. Gobessi, A. Lanzutti, C. Cepek, F. Andreatta, and L. Fedrizzi, Cerium Conversion Coating and Sol-Gel Multilayer System for Corrosion Protection of AA6060, *Surf. Coat. Technol.*, 2016, **287**(3), p 33–43. https://doi.org/10.1016/j.surfcoat.2015.12.059
3. D.K. Heller, W.G. Fahrenholtz, and M.J. O'Keefe, The Effect of Post-Treatment Time and Temperature on Cerium-Based Conversion Coatings on Al 2024-T3, *Corros. Sci.*, 2010, **52**(2), p 360–368. https://doi.org/10.1016/j.corsci.2009.09.023
4. A. Carangelo, M. Curioni, A. Acquesta, T. Monetta, and F. Bellucci, Application of EIS to In Situ Characterization of Hydrothermal Sealing of Anodized Aluminum Alloys: Comparison between Hexavalent Chromium-Based Sealing, Hot Water Sealing and Cerium-Based Sealing, *J. Electrochem. Soc.*, 2016, **163**(10), p C619–C626
5. G. Yoganandan, K. Pradeep Premkumar, and J.N. Balaraju, Evaluation of Corrosion Resistance and Self-Healing Behavior of Zirconium-Cerium Conversion Coating Developed on AA2024 Alloy, *Surf. Coat. Technol.*, 2015, **270**, p 249–258. https://doi.org/10.1016/j.surfcoat.2015.02.049
6. G.E.S.R.G. Buchheit, Jr, and J.P. Moran, Localized Corrosion Behavior of AIloy 2090- The Role of Microstructural Heterogeneity, *Corrosion*, 1990, **46**(8), p 610–617
7. F.H. Scholes, C. Soste, A.E. Hughes, S.G. Hardin, and P.R. Curtis, The Role of Hydrogen Peroxide in the Deposition of Cerium-Based Conversion Coatings, *Appl. Surf. Sci.*, 2006, **253**(4), p 1770–1780
8. B.R.W. Hinton and L. Wilson, The Corrosion Inhibition of Zinc with Cerous Chloride, *Corros. Sci.*, 1989, **29**(8), p 967–985
9. B. Davó, A. Conde, and J.J. De Damborenea, Inhibition of Stress Corrosion Cracking of Alloy AA8090 T-8171 by Addition of Rare Earth Salts, *Corros. Sci.*, 2005, **47**(5), p 1227–1237
10. H. Costenaro, F.M. Queiroz, M. Terada, M.G. Olivier, I. Costa, and H.G. De Melo, Corrosion Protection of AA2524-T3 Anodized in Tartaric-Sulfuric Acid Bath and Protected with Hybrid Sol-Gel Coating, *Key Eng. Mater.*, 2016, **710**, p 210–215
11. W. Izaltino, I. Costa, and C. Regina, Hydrothermal Surface Treatments with Cerium and Glycol Molecules on the AA 2024-T3 Clad Alloy, *Key Eng. Mater.*, 2016, **710**, p 216–221
12. C.E. Castano, M.J.O. Keefe, and W.G. Fahrenholtz, Cerium-Based Oxide Coatings, *Curr. Opin. Solid State Mater. Sci.*, 2015, **19**(2), p 69–76. https://doi.org/10.1016/j.cossms.2014.11.005
13. K.S. Prasad, N.E. Prasad, and A.A. Gokhale, *Microstructure and Precipitate Characteristics of Aluminum-Lithium Alloys*, Elsevier Inc., 2014, p 99–137
14. U. Donatus, M. Terada, C. Ramirez, F. Martins, A. Fatima, S. Bugarin, and I. Costa, On the AA2198-T851 Alloy Microstructure and Its Correlation with Localized Corrosion Behaviour, *Corros. Sci.*, 2018, **131**, p 300–309
15. J. Victor, D.S. Araujo, U. Donatus, F.M. Queiroz, M. Terada, M. Xavier, M. Cavalieri, D. Alencar, and I. Costa, On the Severe Localized Corrosion Susceptibility of the AA2198-T851 Alloy, *Corros. Sci.*, 2018, **133**, p 132–140. https://doi.org/10.1016/j.corsci.2018.01.028
16. J. Victor, D.S. Araujo, A. De Fátima, S. Bugarin, C. De Souza, C. Machado, F.M. Queiroz, M. Terada, A. Astarita, and I. Costa, Thermomechanical Treatment and Corrosion Resistance Correlation in the AA2198 Al – Cu – Li Alloy, *Corros. Eng. Sci. Technol.*, 2019, **54**(7), p 1–12
17. U. Donatus, J.V. de Sousa Araujo, C. de Souza Carvalho Machado, N.V. Vardhan Mogili, R.A. Antunes, and I. Costa, The Effect of Manufacturing Process Induced Near-Surface Deformed Layer on the Corrosion Behaviour of AA2198-T851 Al–Cu– Li Alloy, *Corros. Eng. Sci. Technol.*, 2018, **2782**, p 1–11
18. B.R.W. Hinton, Corrosion Inhibition with Rare Earth Metal Salts, *J. Alloys Compd.*, 1992, **180**, p 15–25
19. K. Hughes, P.R. Hardin, A.E. Wittel, S.G. Miller, Surface Conversion of Aluminum and Aluminum Alloys for Corrosion Protection, *Proc. NACE Meet. Corros. Res. Top. Symp.*, 2000
20. J.I.A. Atkins and P. de Paula, *Physical Chemistry*, 10th ed., Oxford University Press, Oxford, 2014
21. D.D.N. Singh, Corrosion Characteristics of Some Aluminum Alloys in Nitric Acid, *J. Electrochem. Soc*, 1982, **129**(9), p 1869
22. A.E. Hughes, T.G. Harvey, T. Nikpour, T.H. Muster, and S.G. Hardin, Non-Chromate Deoxidation of AA2024-T3 Using Fe(III)-HF-HNO_3, *Surf. Interface Anal.*, 2005, **37**(1), p 15–23